ISSN:2790-1688 Volume-15-(2025)

Design and Simulation of Intelligent Harvesting Device for Daylily

Jiajun Liu [1], Renjie Peng [1], Jingjing Chen [1], Junxiang Ruan [1], Yazi Li [1], and Rong Wang [1, *]

[1] School of Mechanical and Power Engineering, East China University of Science and Technology, Shanghai , 200237, China

Abstract. In view of the prevalent issues of low efficiency, high labor demands, and elevated costs associated with daylily harvesting in most cultivating regions, an automated daylily harvesting device was meticulously designed. This device integrates advanced technologies to address the inherent challenges of daylily harvesting. Initially, SolidWorks was utilized to create a virtual prototype, and Ansys software was employed to simulate the picking action of the end effector, thereby validating the feasibility of its operation. Subsequently, the D-H method was adopted to model the robotic arm, and the Robotics Toolbox in MATLAB was leveraged to construct a digital representation of the robotic arm. This facilitated the analysis of its working interval and trajectory planning simulation. Furthermore, the Yolov7 model was incorporated to recognize daylily images, ensuring the accuracy of the picking process. The outcomes of this research demonstrate that the visual algorithm boasts a high recognition rate, and the chosen robotic arm and end-effector fully meet the design specifications, thereby effectively enhancing the automation level of daylily picking operations.

Keywords: Intelligent Harvesting, Ansys simulation, MATLAB simulation, YOLOv7.

1. Introduction

With the relentless progression of agricultural intelligence, artificial intelligence technologies are orchestrating a profound transformation in traditional agricultural production paradigms [1, 2, 3, 4]. In the realm of fruit and vegetable picking, the seamless amalgamation of deep learning-based object detection algorithms with robotic arm technologies has successfully paved the way for the industrial implementation of automatic picking devices for crops such as strawberries [5] and tomatoes [6]. These innovative advancements have not only markedly elevated production efficiency but have also adeptly alleviated the issue of labor shortages. However, when it comes to daylilies, an economically vital crop, the picking process remains encumbered by numerous technical impediments, necessitating urgent intelligent solutions.

Daylilies, renowned for their rich nutritional content and high economic value, are extensively cultivated across China [7, 8]. Nevertheless, their harvesting period is characterized by high concentration and time sensitivity [9]. Currently, manual harvesting predominates as the primary method. This approach is inherently labor-intensive, inefficient, and falls short in accommodating the demands of large-scale cultivation. As rural labor costs continue to escalate, daylily growers confront mounting economic pressures. Consequently, the development of an efficient, precise, and cost-effective automated daylily picking device holds paramount significance for the sustainable growth of the daylily industry.

The unique characteristics of daylily harvesting, such as the small and densely packed flower buds, delicate stems susceptible to damage, and the complex and ever-changing planting environment, render traditional agricultural robotic technologies inadequate in fulfilling the picking requirements. Thus, this research endeavor devised an automated daylily harvesting device by incorporating the latest advancements in artificial intelligence technology. The device ingeniously amalgamates machine vision, robotic arm control, end-effector design, and independently suspended wheels, with the overarching objective of achieving efficient, precise, and fully automated daylily picking.

2. Design of the Intelligent Harvesting Device for Daylily

2.1 Overall structural design and working principle

The Intelligent Harvesting Device for Daylily is a sophisticated system encompassing four core modules: the mobile platform, the picking device, the machine vision recognition system, and the control system. These modules are intricately integrated to form a cohesive whole, as vividly depicted in Figure 1.

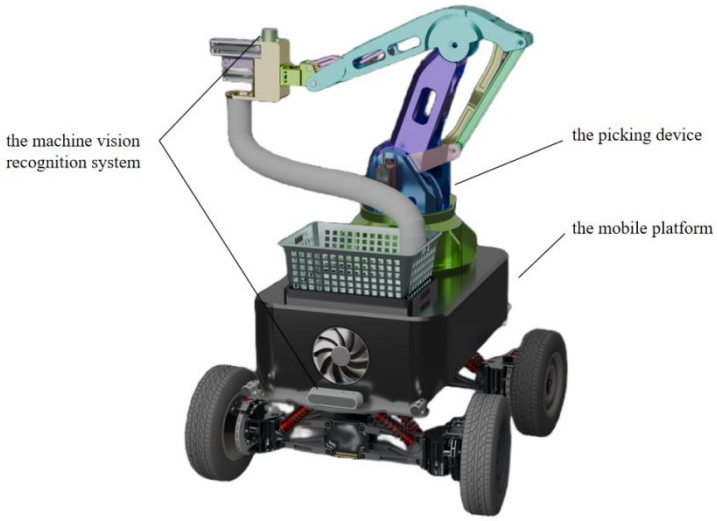

Fig. 1. Overall Structure of the Device

During operation, the device initially positions itself at the picking and collection area. Upon commencement of the task, it follows a pre-set navigation route towards the planting area. The depth camera mounted on the mobile platform, in tandem with real-time road condition data, accurately locates the target daylily plants. Subsequently, the depth camera, integrated with the robotic arm, collaborates with the machine vision recognition system. This synergy facilitates the precise identification of mature daylilies, with the picking coordinate data transmitted in real-time to the central control system.

Thereafter, the control system orchestrates the robotic arm to execute precise picking maneuvers. It meticulously cuts the mature daylilies, which then glide down a dedicated hose and into the collection basket. When the weight of the daylilies in the basket attains a pre-determined threshold, the picking device autonomously returns to the starting position to replace the collection basket. Following the replacement, the device seamlessly resumes operation from the last picking point, ensuring the continuity and high efficiency of the harvesting process.

2.2 Design of the mobile platform

The mobile platform, functioning as the locomotive carrier of the Intelligent Harvesting Device for Daylily, is engineered in the form of a cart. This cart is meticulously designed to accurately position the target area in accordance with operational requirements. The platform integrates the driving mechanism, robotic arm, and the collection basket. Internally, it houses crucial components such as the power supply unit, control center, and depth camera. Ensuring the overall stability of the platform represents a pivotal design consideration.

To accomplish this, the cart employs an independent suspension system configured as a disconnected axle. In this system, the wheels are connected to the chassis through independent suspensions. This ingenious design enables each wheel to move autonomously when subjected to impacts. Consequently, it provides exceptional shock-absorbing capabilities and mitigates the influence of uneven terrains on the robotic arm. Moreover, the system effectively lowers the center of gravity and enhances wheel traction, allowing the wheels to independently adapt to complex

terrains. In summary, the independent suspension system significantly improves the stability and operational efficiency of the cart, thereby contributing to the overall performance of the Intelligent Harvesting Device for Daylily.

2.3 Design of the picking device

The mobile platform, functioning as the locomotive carrier of the Intelligent Harvesting Device for Daylily, is engineered in the form of a cart. This cart is meticulously designed to accurately position the target area in accordance with operational requirements. The platform integrates the driving mechanism, robotic arm, and the collection basket. Internally, it houses crucial components such as the power supply unit, control center, and depth camera. Ensuring the overall stability of the platform represents a pivotal design consideration.

2.3.1 Robotic Arm

The picking process predominantly relies on binocular vision to ascertain the maturity of the daylily, working in conjunction with the robotic arm. Considering the plethora of flowers on each daylily plant, the robotic arm necessitates a high degree of freedom. Therefore, the device employs a linkage joint type mechanism for the arm, comprising four degrees of freedom: rotation at the waist, horizontal extension, vertical pitch, and rotation at the wrist. The specific structure is showcased in Figure 2.

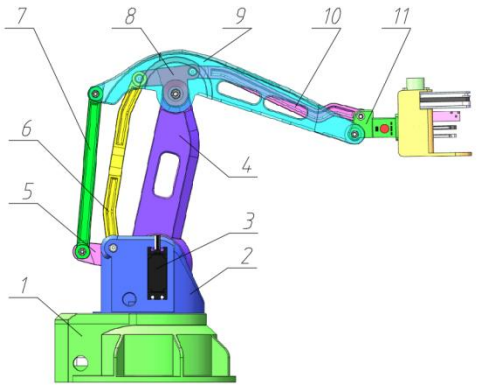

Fig. 2. Linkage Joint Type Robotic Arm

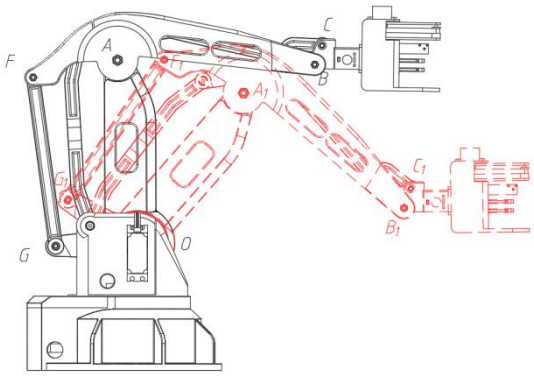

Fig. 3. Robotic Arm Motion Positions

Base: Serves as the foundation of the robotic arm. 2. Waist: Facilitates rotation of the entire arm assembly. 3. Motor: Provides the motive force for arm movement. 4. Upper Arm: Extends horizontally. 5. Lower Arm: Pivots vertically. 6. Adjustment Rod: Fine-tunes the positioning of the lower arm. 7. Lower Arm Linkage: Connects the lower arm to the forearm. 8. Triangular Adjuster: Assists in maintaining the structural integrity of the arm. 9. Forearm: Supports the end effector. 10.

Adjuster Linkage: Fine-tunes the positioning of the forearm. 11. Wrist: Enables rotation of the end effector.

Based on the overall design, pertinent calculations were conducted to select the most suitable components. In practical scenarios, when the forearm is in a horizontal position and the upper arm is vertical, the robotic arm attains its highest point. Conversely, when the mechanism shifts to the position depicted by the dotted line, it reaches its lowest point, with the upper arm forming a 45-degree angle with the horizontal plane. These two extreme positions are illustrated in Figure 3.

The robotic arm components are fashioned from Q235 steel, a low-carbon steel renowned for its exceptional plasticity, toughness, and relatively high strength and hardness. Utilizing SolidWorks software, the mass of each robotic arm component was determined as shown in Table 1.

Table 1. Mass of Each Robotic Arm Component

Number	Name	Mass (kg)
1	Forearm	12.296
2	Lower Arm	3.016
3	Lower Arm Linkage	2.168
4	Upper Arm	12.696
5	Adjustment Rod	2.168
6	Triangular Adjuster	4.752
7	Adjuster Linkage	2.096
8	End Effector	6.520

Force analysis was meticulously conducted when the forearm is in the solid line position, as depicted in Figure 4:

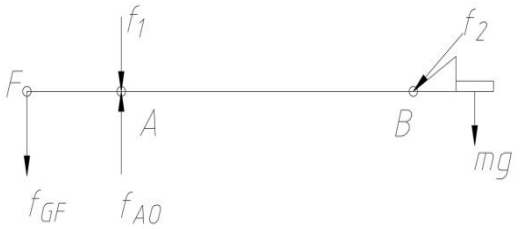

Fig. 4. Forearm Force Diagram

Given the forearm's weight (FB) of 122N and the weight of the end effector (65.2N), the distance from mg to B is 10cm, and the distance from the adjuster linkage to the forearm is 6.4cm. By leveraging these values, the following calculations were performed:

$$mg \times 5 = f \times 6.4 = f_2 \sin 45° \times 6.4 \tag{1}$$

We can get $f_2 = 72.04$N, $f = f_2 \sin 45° = 50.94$N.

Known $|AB| \approx 5|FA|$, by considering the system's equilibrium:

$$f_{gf}|FA| = \frac{2}{3} G_{BF} \times 3|FA| + f \times 5|FA| = 498.7\text{N} \tag{2}$$

The maximum torque on the lower arm is calculated as:

$$M = f_{gf} \times l_{\text{lower arm}} = 498.7 \times 0.15 = 74.805\text{N•m} \tag{3}$$

When the mechanism moves to the position shown in the dotted line, force analysis diagrams for each robotic arm part are shown in Figure 5:

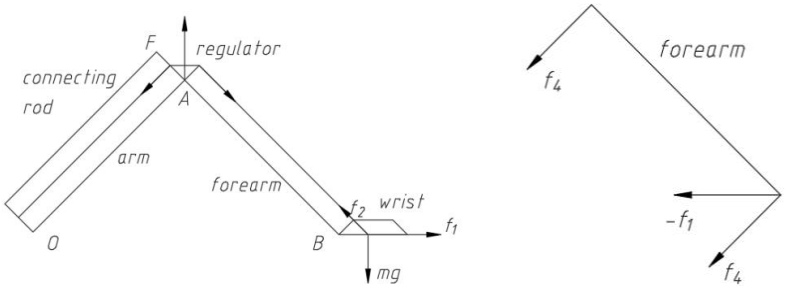

Fig. 5. Force Diagram of Robotic Arm Components

From force equilibrium:

$$-f_1 \times \sin 45° \times |AB| = -mg\sin 45° \times \sin 45° \times |AB| = f_4 \times |FA| \quad (4)$$

We can get $f_4 = 163N$, $-f_2 = f_2 = f_{21} = mg = 65.2N$.

Thus, the combined force at point A is:

$$f_{combinated} = f_{21} \sin 45° + f_4 \sin 45° + mg_{forearm} \approx 283.4N \quad (5)$$

Furthermore, the weight of the arm itself is approximately 127N, |OA|=38cm.

Therefore, the maximum torque on the upper arm's rotational axis when the mechanism reaches the dotted line position is:

$$M_{combinated} = f_{combinated} \times |OA| \sin 45° + \frac{1}{2} mg_{upper\ arm} \sin 45° \approx 121.05N•m \quad (6)$$

2.3.2 Design of the end effector

The end effector comprises a synchronous belt, gripper, and cutting tool. The working principle is as follows: Once the robotic arm reaches the designated position, the synchronous belt, in coordination with non-gear mesh, commences tightening and grips the root of the daylily. The daylily is subsequently pulled closer to the cutting tool and gripper. An infrared sensor, positioned above the gripper, detects when the daylily is in place, prompting the gripper to clamp the stem. The cutting tool then slices the stem, culminating in the picking process. Following the cut, the gripper and synchronous belt open to release the daylily, which plummets into a collection pipe and eventually into the collection basket fixed on the cart. The mechanism diagram is illustrated in Figure 6, and its 3D model is showcased in Figure 7.

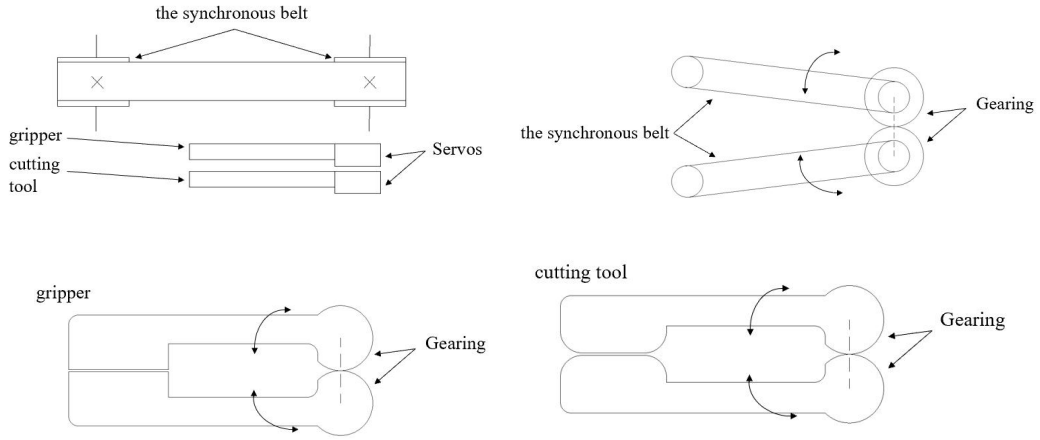

Fig. 6. Mechanism Diagrams of the end effector

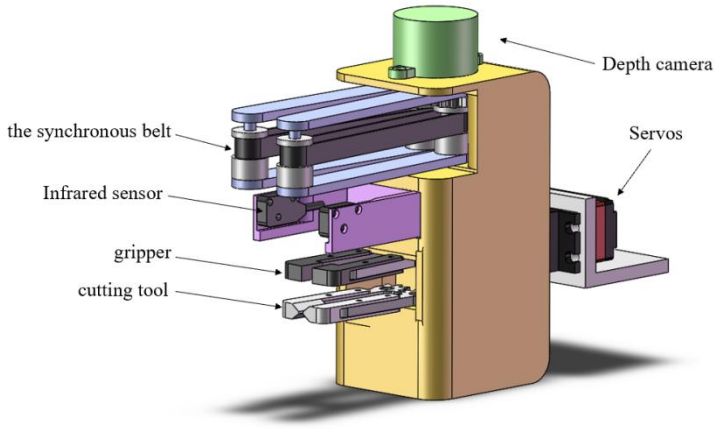

Fig. 7. 3D Model of the end effector

2.3.3 Design of the collection basket

The picked daylilies plummet into the collection basket via a meticulously designed collection pipe attached to the end effector. The bottom of the collection basket is equipped with a pressure sensor to monitor the load in real-time. To ensure operational efficiency while minimizing the cart's energy consumption, a collection pipe was ingeniously designed beneath the robotic arm's end effector. Upon picking, the daylilies directly descend into the basket via the pipe, obviating the need for frequent opening and closing actions of the robotic arm, thereby saving time and significantly enhancing picking efficiency. When the collected daylilies attain a certain weight, the pressure sensor triggers a signal to the microcontroller, prompting the operator to return to the base to replace or empty the collection basket.

2.4 Machine Vision Recognition System

The machine vision recognition system serves dual functions: providing environmental perception and path planning support for the mobile platform, and facilitating precise identification and coordinate positioning of mature daylilies for the picking device, with real-time data feedback to the control system. The latter function will be the focus of the following discussion.

The machine vision recognition system leverages an improved convolutional neural network to achieve automatic identification and detection of daylily targets. It integrates corner detection algorithms and depth camera technology to accomplish precise positioning of daylily picking points.

In machine learning algorithms, to accurately train the recognition model, the target object needs to be labeled to effectively separate it from the background image, as illustrated in Figure 8. In this experiment, the target objects primarily encompass daylily buds and their connection with the flower stems below, the latter being crucial for determining subsequent picking points.

Fig. 8. Example of daylily labeling

Given the limited number of daylily image data, data augmentation was performed by adjusting brightness and image flipping, as depicted in Figure 9, to ensure the training samples are applicable to various scenarios and to enhance the training effect. By simulating light and dark variations in

the scene and augmenting samples from different angles, the accuracy of the trained model's recognition was improved.

(a) Original (b) Brightness adjustment (c) Horizontal flip (d) Rotation

Fig. 9. Dataset Processing

Following annotation and augmentation, the dataset of 2140 training images was generated. These images were labeled using PyCharm and randomly partitioned into training (1498 images), validation (321 images), and test sets (321 images) at a 7:1.5:1.5 ratio. Given the complex background interference and occlusion issues inherent in daylily bud recognition, along with the similarity in color and morphology between mature and immature buds, both the Yolov7 and Faster-RCNN networks were selected for comparative evaluation. Figure 10 presents the Faster-RCNN recognition results, while Figure 11 displays the Yolov7 recognition results.

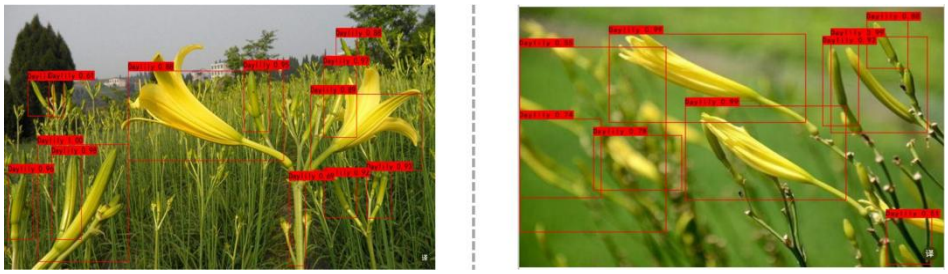

Fig. 10. Faster-RCNN Network Architecture

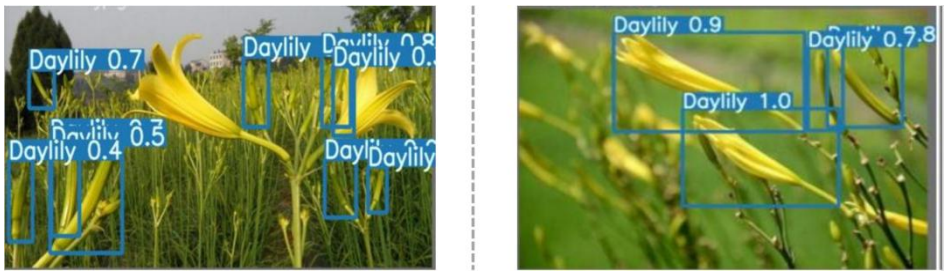

Fig. 11. YOLOv7 Network Architecture

The results demonstrate that the Yolov7 network exhibits superior detection capabilities in complex environmental backgrounds, enabling comprehensive target recognition. It can effectively identify mature daylily buds even under severe occlusion between buds. Furthermore, Yolov7 significantly outperforms Faster-RCNN in detection speed, leading to the final selection of the Yolov7 algorithm.

The model's performance was evaluated using metrics including Precision, Recall, and mean Average Precision (mAP).

Precision is defined as the ratio of correctly detected targets (True Positives, TP) to all detection results (TP + False Positives, FP).

$$\text{Precision} = \frac{\text{TP}}{\text{TP+FP}} \quad (7)$$

High precision indicates that the model exhibits a low rate of false positives.

Recall is defined as the ratio of correctly identified targets (TP) to the total number of actual targets present (TP + False Negatives, FN).

$$\text{Recall} = \frac{\text{TP}}{\text{TP+FN}} \quad (8)$$

High recall indicates that the model has fewer missed detections (false negatives).

In object detection tasks, mAP (mean Average Precision) is a key metric for evaluating model performance, comprehensively reflecting the model's detection capabilities across different categories, confidence thresholds, and Intersection over Union (IoU) requirements.

$$\text{AP} = \int_0^1 \text{P(r)dr} \quad (9)$$

For single-class tasks: mAP = AP.

The current model achieves a precision of 0.84, a recall of 0.758, and a mean Average Precision (mAP@0.5) of 0.81. This indicates a low rate of false positives and a high degree of confidence in the detection results. However, some instances of missed detections are observed, particularly when the daylily targets are small or heavily occluded. Despite this, in practical application scenarios, the model can identify the majority of daylilies within the camera's field of view in a single pass. Furthermore, the multi-angle movement and re-examination capabilities of the harvesting device are employed to mitigate missed detections.

The key to automated daylily harvesting lies in the precise localization of the harvesting point. This step is crucial for protecting immature flower buds and maintaining the regenerative capacity of the plant. The harvesting point should be precisely set at the junction of the flower calyx and the peduncle, ensuring that only the stem is harvested without damaging the branch. This connection area is defined as the Region of Interest (ROI) for the daylily, specifically encompassing the upper portion of the perianth tube (a part of the calyx) and the lower portion of the scape (part of the peduncle). The length of the upper portion of the perianth tube ranges from approximately 35 to 45 cm, while the scape length varies between 20 and 30 cm. The mathematical representation of the ROI can be expressed as:

$$h = 0.62(m_{max} + m_{min}) \quad (10)$$

$$b = 0.43(n_{max} + n_{min}) \quad (11)$$

Within formulae, h represents height, b represents thickness, m denotes the pixel value corresponding to the height of the region of interest (ROI), and n denotes the pixel value corresponding to the width of the ROI.

To achieve automated identification of harvesting points, image processing of the daylily connections is required. The initial step involves grayscale conversion to facilitate subsequent corner detection. The Harris corner detection algorithm was selected due to its effectiveness in identifying corners within an image. This algorithm is based on the analysis of image grayscale variations, locating corners by computing a corner response function for each pixel.

The core of the Harris algorithm involves approximating image grayscale variations through a Taylor series expansion, constructing a structure matrix to describe this variation. For any pixel in the image, when a small movement occurs in its surrounding window (with displacements u and v in the x and y directions, respectively), the autocorrelation function of the grayscale variation can be expressed as:

$$E(u,v) = \sum_{x,y} w(x,y)[I(x+u, y+v) - I(x,y)]^2 \quad (12)$$

Within this formula, $w(x, y)$ represents the weighting function, which can be expressed as a constant or a Gaussian weighting function; $I(x + u, y + v)$ denotes the pixel grayscale value after image translation; and $I(x, y)$ represents the pixel grayscale value before image movement.

By performing a first-order approximation of$I(x + u, y + v)$using a two-dimensional Taylor series expansion, the expression for the structure matrix can be derived. To simplify the computation, the corner response function R is introduced, which is used to determine whether a pixel is a corner:

$$R = \det(M) - k\big(\mathrm{tr}(M)\big)^2 = \lambda_1\lambda_2 - k(\lambda_1 + \lambda_2)^2 \quad (13)$$

The parameter k represents an empirically determined constant, with a typical range of 0.04 to 0.06. The variables λ_1 and λ_2 correspond to the eigenvalues of matrix M.

The calculated response value, denoted as R, is subsequently compared against a predefined threshold, T. A point is classified as a corner if R is greater than or equal to T; otherwise, it is not. Based on this theoretical framework, a corner analysis was performed on the daylily connection points, and the results are presented in Figure 12.

Fig. 12. Corner detection analysis results

2.5 Electrical Control System

As the central core of the device, the control system comprises a power module, main control board, navigation system, and other critical components. It efficiently coordinates the operation of various modules by issuing precise commands in real time, ensuring stable and high-performance execution of harvesting tasks.

The electrical control system of the intelligent daylily harvesting vehicle is centered on the STM32F103C8T6 microcontroller. It employs PWM signals to govern multiple servo motors, DC motors, and stepper motors, enabling precise control of the robotic arm, clamping device, the conveyor belt, chassis, and wheels. The system supports two operational modes: autonomous harvesting based on three-dimensional coordinate data transmitted from the host computer, and manual control via a Bluetooth module.

In the DC motor drive subsystem, a speed measurement module is integrated to monitor rotational speeds. The acquired data is fed back to the STM32 minimum system board to achieve closed-loop control.

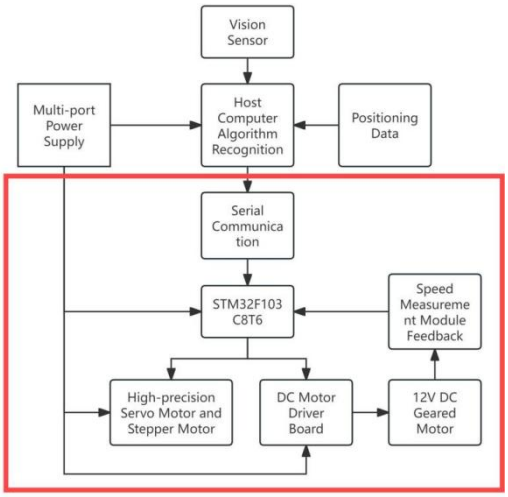

Fig. 13. Overall Architecture of the Electrical Control System

As illustrated in Figure 13 (red highlighted section), the architecture of the electrical control system features an integrated multi-port power supply capable of delivering multiple voltage outputs. This design enables unified power management for the STM32 control board, servo motors, and DC motors through a single power source.

3. Simulation Analysis of the Movement of the Picking Mechanism

In the simulation analysis of the motion of the daylily picking mechanism, the mass of the daylily has a crucial influence on the pressure exerted by the fixture. In order to accurately measure the average weight of daylilies, a high-precision electronic balance was used to measure and the mass data of 70 daylilies were recorded, and the average mass of daylilies was 2.174 grams.

In order to verify whether the fixture will cause damage during the clamping of daylily, a three-dimensional model of the end effector and daylily was established by using Solidworks software. Subsequently, the Transient Structure Simulation was performed on the situation of the daylily being clamped by the fixture using the Ansys Workbench platform. The purpose of this step is to observe the deformation of the daylily when it is subjected to pressure, so as to determine whether the pressure of the fixture will cause the daylily to be significantly deformed or even damaged.

After the model is imported, in the Mechanical module, the model material is defined. The material of the end effector is set to structural steel, and its Young's modulus and Poisson's ratio are set at 2×105MPa and 0.3, respectively. The material properties of daylily were set as Young's modulus 2.9 MPa, Poisson's ratio 0.4, and density 0.27 g/cm^3 . Since the imitation of Allah this time focuses on the deformation of the yellow cauliflower when clamping, the jig and the yellow cauliflower are set as flexible bodies, while the rest of the parts are treated as rigid bodies.

According to the actual needs of simulation and the specific situation of clamping, a rotary motion pair is arranged in the fixture part, and other parts and daylily are set to a fixed state, as shown in Figure 14. At the same time, a frictional contact relationship was established between the fixture and the daylily, in which the surface of the fixture was defined as the contact surface, the surface of the daylily was the target surface, and the friction coefficient was set to 0.3 after careful consideration.

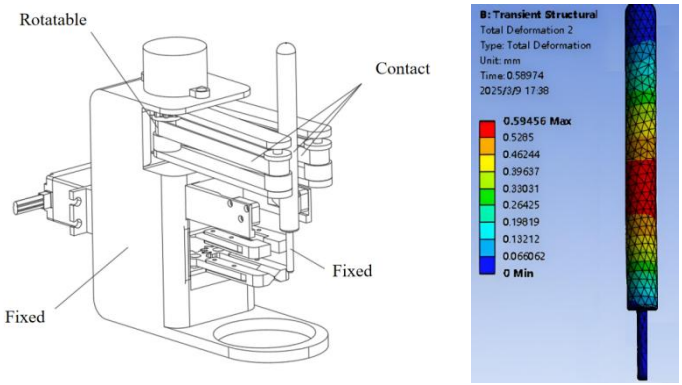

Fig. 14. Schematic diagram of constraints

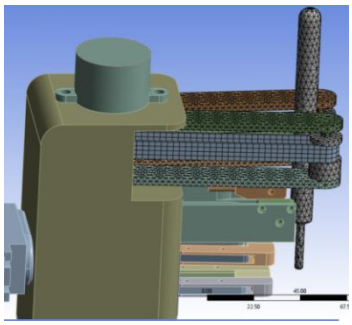

Fig. 15. Network division diagram Total Deformation Diagram of Daylily

The quality of the meshing has a crucial impact on the accuracy of the simulation results, and in order to ensure the speed of the calculation while taking into account the accuracy of the simulation, only the fixture part and the daylily were meshed, while the other parts were not processed. In order to ensure the accuracy of the meshing, the grid size is set to be relatively dense, the cell size is set to 3mm, and the rest of the settings are left default. After careful meshing, the final number of generated grid cells totaled 18,647 and the number of nodes totaled 38,277,the grid division is shown in Figure 15.

In the Transient module, load options are inserted, and the loading object is set to the fixture section, while the pressure is precisely calculated and set based on the average mass and coefficient of friction of the daylily. To ensure that the daylily can be clamped stably, the clamping pressure is set to be slightly greater than the minimum required pressure value, i.e. 0.1 N.

Enabled automatic time increment steps in the analysis settings, and changed the definition of step control to substeps, with the initial and minimum substeps set to 10 and the maximum substeps set to 50. Once the setup is complete, start the solve process.

After the calculation is completed, the total deformation of daylily is checked, and the result is shown in Figure 16. From the simulation results, it can be seen that the maximum deformation occurs at the contact part with the fixture, the maximum deformation is 0.59mm, and the diameter of the daylily bud part is about 10mm. Compared with the size of the daylily, the deformation caused by the clamping pressure to the daylily is small, and it will not cause damage to the daylily.

4. Kinematic Analysis of the Robotic Arm

4.1 Establishing the Forward Kinematic Model of the Robotic Arm

The forward kinematics of the robotic arm refers to deriving a set of equations related to the robot's configuration. By substituting the link parameters and joint angles into these equations, the robot's pose can be determined[10].

To determine the relative motion relationship between the end effector and each link of the robotic arm, the Denavit-Hartenberg (D-H) parameter method is used to establish the coordinate systems for each joint[11,12]. The main parameters of the robotic arm and the corresponding coordinate system diagram are shown in Figure 16.

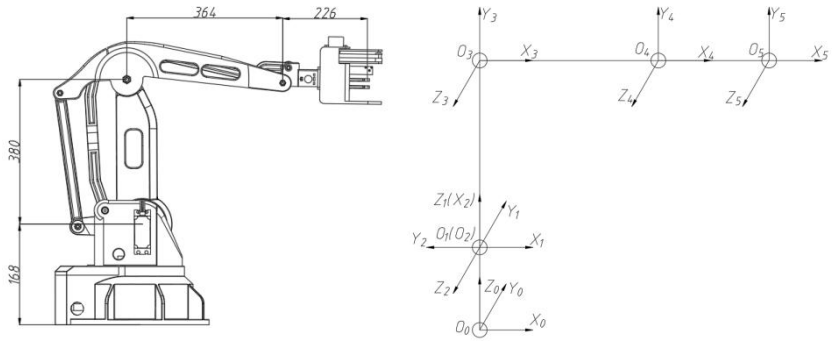

Fig. 16. Main Parameters and Coordinate System Diagram of the Robotic Arm

It is defined that α i-1 is the link twist angle; ai-1 is the link length; θ i is the joint angle; di is the link offset. The D-H parameters are shown in Table 2.

Table 2. D-H Parameter Table

i	ai-1	αi-1	di	θiInitial	Range of joint rotation angles
1	0	0	168	0	[-180°,180°]
2	0	pi/2	0	pi/2	[-60°,30°]
3	380	0	0	-pi/2	[-51°,31°]
4	364	0	0	0	-(θ2+θ3)
5	226	0	0	0	[-180°,180°]

4.2 Forward Kinematic Equations

Using the homogeneous transformation matrix theory of the D-H parameter method and mathematical computations, the general 4 × 4 matrix for the coordinate system transformation between adjacent links can be obtained:

$$ {}^{i-1}_{i}T = \begin{bmatrix} \cos\theta_i & -\sin\theta_i & 0 & a_{i-1} \\ \sin\theta_i\cos\alpha_{i-1} & \cos\theta_i\cos\alpha_{i-1} & -\sin\alpha_{i-1} & -d_i\sin\alpha_{i-1} \\ \sin\theta_i\sin\alpha_{i-1} & \cos\theta_i\sin\alpha_{i-1} & \cos\alpha_{i-1} & d_i\cos\alpha_{i-1} \\ 0 & 0 & 0 & 1 \end{bmatrix} \quad (14) $$

By substituting the link parameters from the D-H table into the above formula, the transformation matrices for each link, ${}^{0}_{1}T$、${}^{1}_{2}T$、${}^{2}_{3}T$、${}^{3}_{4}T$、${}^{4}_{5}T$, can be obtained.

By multiplying the transformation matrices for all links, the transformation matrix of the end effector relative to the base coordinate system can be obtained ${}^{0}_{5}T = {}^{0}_{1}T{}^{1}_{2}T{}^{2}_{3}T{}^{3}_{4}T{}^{4}_{5}T$.

$$ {}^{0}_{5}T = \begin{bmatrix} n_x & o_x & a_x & p_x \\ n_y & o_y & a_y & p_y \\ n_z & o_z & a_z & p_z \\ 0 & 0 & 0 & 1 \end{bmatrix} \quad (15) $$

$$ p_x = 380c_1c_2 + 226c_{23}(c_1c_2c_3 - c_1s_2s_3) + 226s_{23}(c_1c_2s_3 + c_1c_3s_2) + 364c_1c_2c_3 - 364c_1s_2s_3 \quad (16) $$

$$ p_y = 380c_2s_1 + 226c_{23}(c_2c_3s_1 - s_1s_2s_3) + 226s_{23}(c_2s_1s_3 + c_3s_1s_2) + 364c_2c_3s_1 - 364s_1s_2s_3 \quad (17) $$

$$ p_z = 380s_2 + 364c_2s_3 + 364c_3s_2 + 226c_{23}(c_2s_3 + c_3s_2) - 226s_{23}(c_2c_3 - s_2s_3) + 168 \quad (18) $$

In the above equation, si represents the abbreviation for sin θ i, ci represents the abbreviation for cos θ i, sij represents the abbreviation for sin(θ i+ θ j), and cij represents the abbreviation for cos(θ i+ θ j). The matrix ${}^{0}_{5}T$describes the relationship between the coordinates and orientation of the end-effector coordinate system and the base coordinate system of the robotic arm. The parameters n, o, a reflect the orientation changes of the end-effector in the spatial coordinate system, while the parameter p reflects the changes in the three-dimensional coordinates of the end-effector in the spatial reference coordinate system.

4.3 Forward Kinematics Simulation

Using Matlab’ s Robotics Toolbox, Link, and SerialLink functions, the motion model of the robotic arm is established. The D-H parameters from the table are substituted into Matlab for simulation. The simulation model of the harvesting robotic arm is shown in Figure 17.

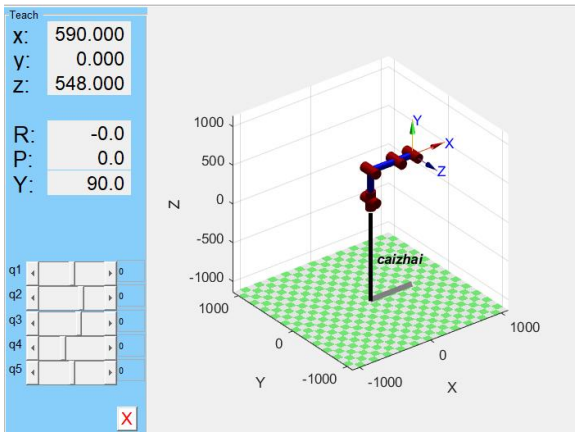

Fig. 17. Simulation Model of the Harvesting Robotic Arm

In the figure, x, y and z represent the spatial position coordinates of the end-effector, and R, P, Y represent the rotation angles of the end-effector coordinate system relative to the space base coordinate system. q1 to q5 are the joint angles of the robotic arm, and by adjusting the values of q1 to q5, the position of the end-effector can be changed. By substituting the initial joint angles θ 1=0、 θ 2=pi/2、 θ 3=-pi/2、 θ 4=0、 θ 5=0 into the transformation matrix ${}^{0}_{5}T$, we get:

$$ {}^{0}_{5}T = \begin{bmatrix} 1 & 0 & 0 & 590 \\ 0 & 0 & -1 & 0 \\ 0 & 1 & 0 & 548 \\ 0 & 0 & 0 & 1 \end{bmatrix} \tag{19} $$

The computed matrix results are consistent with the Matlab simulation results, verifying the correctness of the forward kinematic model.

4.4 Robotic Arm Workspace Simulation

The workspace of the robotic arm is the collection of all the spatial points that the end effector can reach. The workspace is solved using the Monte Carlo method. The `rand` function is used to randomly select the rotation angles of each joint. After determining the joint angles, the end effector of the robotic arm reaches a random point. After 30,000 iterations, 30,000 random points are generated, and the workspace range,the workspace in the XY plane and the workspace in the XZ plane of the robotic arm is plotted in Matlab, as shown in Figure 18.

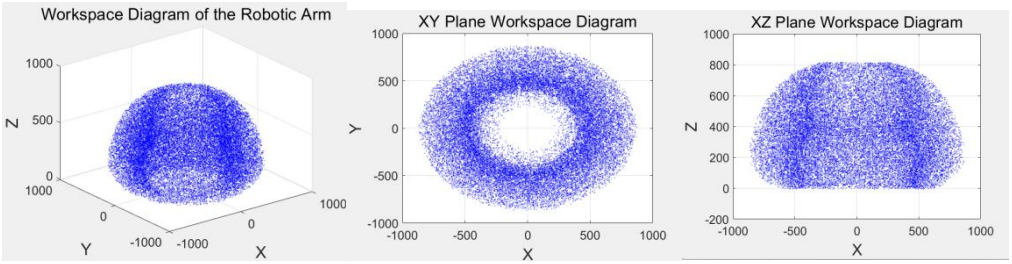

Fig. 18. Workspace Diagram of the Robotic Arm

As shown in the figure, the harvesting robotic arm can reach a range of approximately (-900, 900) along the X-axis, a range of approximately (-900, 900) along the Y-axis, and a range of approximately (0, 800) along the Z-axis. With the forward and backward movement of the platform, this can meet the space requirements for harvesting daylilies.

Based on research on the characteristics of daylily plants, the average height of the plants is about 160 cm. The workspace of this harvesting robotic arm is approximately a sphere with a radius of 90 cm. Adding the height of the mobile platform, the end effector of the robotic arm can perform harvesting at every point on the daylily plant, verifying the feasibility of using this robotic arm for daylily harvesting.

5. Conclusions

1) Based on the cultivation characteristics of daylilies, an intelligent harvesting device was designed to integrate the advantages of a high-stability mobile platform, a high-precision machine vision recognition system, and a non-destructive harvesting mechanism, thereby significantly improving the efficiency and automation level of daylily harvesting operations.

2) A three-dimensional model of the daylily harvesting manipulator was established, with material parameters and simulation boundary conditions defined. Finite element simulations were conducted using Ansys software. Simulation analysis and numerical calculations demonstrated that a clamping force of 0.1 N achieves non-destructive harvesting of daylilies.

3) The working range of the robotic arm was validated through simulation. A forward kinematics model was developed, and its workspace was simulated. Results indicate that the robotic arm's workspace approximates a spherical region with a radius of 90 cm, fully satisfying the spatial requirements for harvesting operations.

References

[1] Eli-Chukwu N C. Applications of artificial intelligence in agriculture: A review[J]. Engineering, Technology & Applied Science Research, 2019, 9(4).

[2] Bannerjee G, Sarkar U, Das S, et al. Artificial intelligence in agriculture: A literature survey[J]. international Journal of Scientific Research in computer Science applications and Management Studies, 2018, 7(3): 1-6.

[3] Jha K, Doshi A, Patel P, et al. A comprehensive review on automation in agriculture using artificial intelligence[J]. Artificial Intelligence in Agriculture, 2019, 2: 1-12.

[4] Sharma R. Artificial intelligence in agriculture: a review[C]//2021 5th international conference on intelligent computing and control systems (ICICCS). IEEE, 2021: 937-942.

[5] Zheng C, Abd-Elrahman A, Whitaker V. Remote sensing and machine learning in crop phenotyping and management, with an emphasis on applications in strawberry farming[J]. Remote Sensing, 2021, 13(3): 531.

[6] Lee J, Nazki H, Baek J, et al. Artificial intelligence approach for tomato detection and mass estimation in precision agriculture[J]. Sustainability, 2020, 12(21): 9138.

[7] Gulia S K, Singh B P, Carter J, et al. Daylily: botany, propagation, breeding[J]. 2009.

[8] Lay-Yee M, Stead A D, Reid M S. Flower senescence in daylily (Hemerocallis)[J]. Physiologia Plantarum, 1992, 86(2): 308-314.

[9] Zhao J, Dai F, Zhang T. System Design of Daylily Picking Robot[J]. Journal of Robotics, Networking and Artificial Life, 2022, 9(1): 20-24.

[10] Cai J, Deng J, Zhang W, et al. Modeling Method of Autonomous Robot Manipulator Based on D-H Algorithm[J]. Mobile Information Systems, 2021, 2021(1): 4448648.

[11] Mohammed A A, Sunar M. Kinematics modeling of a 4-DOF robotic arm[C]//2015 International Conference on Control, Automation and Robotics. IEEE, 2015: 87-91.

[12] Li Y B, Li T J, Zhu H F, et al. Comparative analysis of the kinematics solution based on the DH method and screw theory[J]. Mathematical Problems in Engineering, 2021, 2021(1): 6694621.